ICAS 2016
30th Congress of the International Council of the Aeronautical Sciences
DCC, Daejeon, Korea ; September 25-30, 2016

THE EFFECTS OF BODY AERODYNAMICS ON THE DYNAMIC STABILITY OF INSECT FLIGHT

Anh Tuan Nguyen, Joong-Kwan Kim, Jae-Hung Han
Department of Aerospace Engineering, KAIST
Daejeon 305-701, Republic of Korea

Keywords: *insect flight, panel code, multibody dynamics*

Abstract

This study investigates the effects of body aerodynamics on the longitudinal dynamic stability characteristics of insect flight. The aerodynamic model, which comprises the panel method and the extended unsteady vortex-lattice method, is used to compute the aerodynamic forces acting on the body and the wings, respectively. The nonlinear equations of motion of the insect are solved by a multibody dynamics code. The trim conditions are found by the trim search algorithm. The dynamic modal structures of the insect motion, including eigenvectors and eigenvalues are obtained to indicate the effects of the body aerodynamics on the dynamic stability. The results of the study show that the effects of the body aerodynamics on the dynamic stability and the trim conditions of insect flight tend to be more significant when the flight speed increases.

1 Introduction

Insect flight has drawn researchers' interests for the past several decades. Learning the way insects fly is beneficial for the future designs of micro air vehicles. Unlike other types of aircraft, insects use only a pair or two pairs of wings to control their flight. Because of this flight characteristic, researchers have made many attempts to understand the dynamic stability of insect flight [1-7]. However, in these studies, the contribution of the body aerodynamics has been usually neglected. Generally, this assumption is adequate to hovering and low-speed flight. Nevertheless, in fast flight, the contribution of body aerodynamic may not be small; hence, this force component needs to be included to ensure the accuracy of the results.

The purpose of this study is to analyze the effects of the body aerodynamics on the dynamic flight stability of a hawkmoth *Manduca sexta* model with respect to various flight speeds. The aerodynamic model used in this study is the combination of the panel method (PM) and the extended unsteady vortex-lattice method (UVLM). Both of these methods are based on the potential flow theory. The PM is applied to compute the aerodynamic force on the body; while the extended UVLM is used for the aerodynamics of the flapping wings. The extended UVLM proposed by Nguyen et al. [8] can include the effect of the leading-edge vortices appearing on insect wings, and overcome the instability due to wing-wake interaction. To solve the nonlinear equations of motion, the multibody dynamics code, which is available in the *MSC. Adams* software, is employed. The trimmed flight states are obtained by the trim search algorithm [7]. The eigenvalues and eigenvectors of the linearized dynamic system are computed and analyzed to indicate the effects of the body aerodynamics on the longitudinal dynamic characteristics of insect flight.

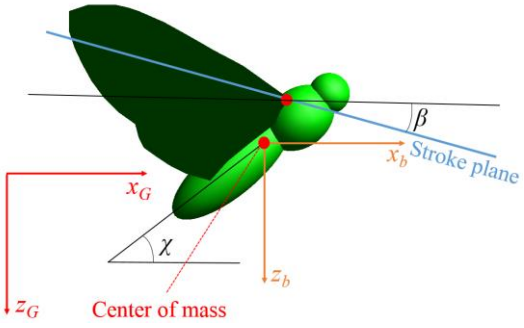

Fig. 1. Insect model

2 Methodology

2.1 Insect Model

The insect model used in this study features the hawkmoth *Manduca sexta* with mass properties and dimensions similar to those from [6]. The insect model consists of a body and two wings (Fig. 1). In the trimmed flight, the body-fixed coordinate system [x_b y_b z_b] and the ground-fixed coordinate system [x_G y_G z_G] have the same orientation as shown in Fig. 1. The stroke plane angle and body angle are denoted by β and χ, respectively.

The wing kinematics parameters and the values of β and χ are based on the measurement data of the real hawkmoth *Manduca sexta* [9].

2.2 Aerodynamic Model

As mentioned in the introduction section, the PM and extended UVLM were used to compute the aerodynamic forces acting on the body and the wings, respectively. This section will present the descriptions of these methods.

2.2.1 Panel Method

The PM used in this study is similar to that presented by Katz and Plotkin [10]. The PM is based on the potential flow theory, which assumes that 1) the flow is attached, 2) viscous effects are insignificant and ignored, 3) the flow is irrotational, which means there is no vorticity everywhere in the computational domain except for solid-body surfaces and wake sheets. According to Dudley [11], hawkmoth *Manduca sexta* is amongst insect species that have the most streamlined bodies; thus, it is possible to apply the PM by assuming that there are no vortices shed from the body.

Let Φ the velocity potential in the ground-fixed coordinate system, then the boundary conditions of the problem are given as

$$\lim_{|\boldsymbol{r}|\to\infty} \nabla\Phi = 0 \tag{1}$$

$$\left(\nabla\Phi - \boldsymbol{v}_b\right)\cdot\boldsymbol{n} = 0 \tag{2}$$

$$\Phi_i = const \tag{3}$$

where, $\boldsymbol{r}$, $\boldsymbol{v}_b$, $\boldsymbol{n}$, and Φ_i are the position vector, the local velocity of the body, the local normal vector of the body surface, and the velocity potential inside the body, respectively. Equations (1-3) are corresponding to the far-field boundary condition, the Neumann boundary condition, and the Dirichlet boundary condition, respectively. The far-filed boundary condition assures the zero flow velocities in the far field. The Neumann boundary condition assures that the local flow velocity relative to the body surface is parallel to the body surface, which means the flow does not penetrate into the body. The Dirichlet boundary condition guarantees the constant velocity potential inside the body.

According to the potential flow theory, for low-speed flows, the governing equation of the aerodynamic problem can be reduced to the Laplace equation of the velocity potential Φ [10]:

$$\Delta\Phi = 0 \tag{4}$$

Applying the third Green's identity, the solution of Eq. (4) at an arbitrary point P in the computational domain could be given as [10]

$$\Phi(P) = -\frac{1}{4\pi}\int_{S_b}\left[\sigma\left(\frac{1}{\boldsymbol{r}}\right) - \mu\boldsymbol{n}\cdot\nabla\left(\frac{1}{\boldsymbol{r}}\right)\right]dS + \frac{1}{4\pi}\int_{S_w}\mu\boldsymbol{n}\cdot\nabla\left(\frac{1}{\boldsymbol{r}}\right)dS \tag{5}$$

where, S_b and S_w are the body and wake sheet surfaces, respectively. σ and μ are called source and doublet elements. The expression of σ is

$$\sigma = \frac{\partial\Phi}{\partial n} - \frac{\partial\Phi_i}{\partial n} \tag{6}$$

The doublet elements μ on the body surface are given as

$$\mu = \Phi_i - \Phi \tag{7}$$

However, on the wake sheets, the doublet elements are

$$\mu = \Phi_l - \Phi_u \tag{8}$$

Here, Φ_l and Φ_u are the velocity potentials on the lower and upper surfaces of the wake sheets, respectively.

From Eq. (3), it follows that $\frac{\partial \Phi_i}{\partial n} = 0$. Therefore, in light of Eqs. (2) and (6), the source elements σ are determined as

$$\sigma = \boldsymbol{v}_b \cdot \boldsymbol{n} \tag{9}$$

Now, the body is divided into triangular and quadrilateral panels. On each panel we place a source element σ and a doublet element μ. The values of the source elements are given by Eq. (9). In order to determine the values of the doublet elements, we form a system of algebraic equations based on the Dirichlet boundary condition [Eq. (3)]. It is possible to set the constant in Eq. (3) to be zero. For bodies with sharp trailing edges, the values of doublet elements on wake sheets could be determined by the Kutta condition, which requires all vortices along sharp trailing edges to leave these edges and form wakes. Wakes are assumed to transport with local flow velocities.

In this study, the vortex-core growth model, which was introduced by Nguyen et al. [8], is employed to overcome body-wake and wing-wake interactions. According to Nguyen et al., wakes consisting of doublet elements could be converted to the system of vortex lines whose core radius increases with time. This technique helps to avoid the singularities due to wing-wake and body-wake interactions. However, it may cause some difficulties while computing the velocity potential induced by wakes. To solve this problem, we can determine the velocity potential due to wakes by the integration of the wake-induced velocity along an arbitrary integral path 1-2:

$$\Phi_{wake} = \int_1^2 \boldsymbol{v}_{wake} d\boldsymbol{s} \tag{10}$$

where, $\boldsymbol{v}_{wake}$ is the wake-induced velocity. In this integral, point 1 is assumed to be in the far-field, and point 2 is chosen at the position, where we need to determine the velocity potential.

The pressure on the body surface is computed by the modified Bernoulli equation:

$$p_{ref} - p = \rho\left[\frac{1}{2}\left(\nabla\Phi\right)^2 + \boldsymbol{v}_{ref} \cdot \nabla\Phi + \frac{\partial\Phi}{\partial t}\right] \tag{11}$$

where, ρ is the air density; p_{ref} is the far-field reference pressure; $\boldsymbol{v}_{ref}$ is the reference velocity, which is equal to the local velocity of the body. The aerodynamic force on a panel is computed as

$$\Delta\boldsymbol{F} = \left(p_{ref} - p\right)\Delta S\,\boldsymbol{n} \tag{12}$$

where, ΔS is the area of the panel.

2.2.2 Extended Unsteady Vortex-Lattice Method

The PM presented in section 3.3.1 may be applied to bluff bodies. However, for the thin wings of the insect model, we need to use the unsteady vortex-lattice method (UVLM). In fact, the UVLM is a reduced version of the PM. For thin objects like insect wings, the lower and upper surfaces coincide with each other, and they have the opposite normal vectors. Therefore, the source elements on the lower and upper surfaces computed by Eq. (6) have the opposite signs; thus, they will cancel out each other. Hence, for the UVLM, source elements are unnecessary.

Similarly, the upper and lower doublet elements are combined to form a unique one. Due to the equivalence between a doublet element and a vortex ring [10], it is possible to replace the combined doublet elements by the system of vortex rings. The circulation values of the vortex rings are found by solving the system of algebraic equations that are formed by the no-penetration boundary condition on the aerodynamic panels.

The UVLM in this study is extended by including the leading-edge suction analogy model, which was developed by Nguyen et al. [8] to consider the effects of the leading-edge vortices. We assume that the leading-edge vortices on insect wings have a spiral form, similar to that on a delta wing. Therefore, these vortices provide an extra normal force component in a similar way to that of the suction force. More details of the extended UVLM can be found in [8].

2.3 Equations of Motion and Trim Search Algorithm

2.3.1 Nonlinear Equations of Motion

The equations of flapping-wing insect motion are highly nonlinear, and they can be expressed in the following form [1]:

$$ {}_b\mathbf{F}_A + m\,{}_b\mathbf{g} = m({}_b\dot{\mathbf{V}}_{cg} + {}_b\boldsymbol{\omega}_{bd} \times {}_b\mathbf{V}_{cg}) + \mathbf{a}_1 + \mathbf{b}_1 \quad (13) $$

$$ {}_b\mathbf{M}_A = {}_b\boldsymbol{\omega}_{bd} \times \left({}_b\mathbf{I}_{bd} + \mathbf{c}_2\right) {}_b\boldsymbol{\omega}_{bd} + {}_b\mathbf{I}_{bd}\,{}_b\dot{\boldsymbol{\omega}}_{bd} + \mathbf{a}_2 + \mathbf{b}_2 \quad (14) $$

Here, ${}_b\mathbf{F}_A$ and ${}_b\mathbf{M}_A$ are the aerodynamic force and moment, respectively; m is the mass of the model; ${}_b\mathbf{g}$ is the gravitational acceleration; ${}_b\mathbf{V}_{cg}$ and ${}_b\boldsymbol{\omega}_{bd}$ are the velocity of the body center and the angular velocity of the body, respectively; ${}_b\mathbf{I}_{bd}$ is the inertial moment tensor of the body. According to [1], $\mathbf{a}_1$ represents the contributions of the weight of the wings and the inertial force of the wings due to the body motion; $\mathbf{a}_2$ represents the contributions of the moments produced by the weight of the wings and by the inertial forces of the wings due to the body motion; $\mathbf{b}_1$ and $\mathbf{b}_2$ are related to the inertial forces and moments of the wings due to the flapping motion. The subscript b refers to the body-fixed coordinate system.

In this study, the nonlinear equations of motion in Eqs. (13) and (14) are solved using the multibody dynamics solver of the *MSC. Adams* software. The aerodynamic force and moment ${}_b\mathbf{F}_A$ and ${}_b\mathbf{M}_A$ are computed by the aerodynamic model presented in section 2.2, and exported to the *MSC. Adams* environment. More details of this multibody dynamics solver are given in [6,7].

2.3.2 Trim Search Algorithm

Before studying the dynamic flight stability of the insect model, it is important to find the trim conditions. In this study, the trim conditions are found by the gradient-based trim search algorithm introduced by Kim et al. [7]. Three parameters, including the flapping frequency f, the mean values of the sweep angle $\bar{\phi}$ and the rotation angle $\bar{\alpha}$, are adjusted to obtain the trim conditions. The sweep angle ϕ and the rotation angle α are amongst the set of the Euler angles, which were defined in [8], to determine the position of the wings.

According to this algorithm, the trim search program has to run many iterations until the rigorous criteria of the trim conditions are satisfied. After each iteration, the initial velocity of the model, and an external offset force applying to the model need to be updated to balance the model. The offset force is then replaced by the change in the wing kinematics through the adjustments in the three parameters f, $\bar{\phi}$, and $\bar{\alpha}$. These adjustments are computed through a matrix consisting of the derivatives of the aerodynamic force and moment with respect to the wing kinematics parameters. The detailed descriptions of the trim search algorithm may be found in [7].

2.3.3 Linearized Equations of Motion

If we assume that the flapping frequency of the wings is much higher than the natural frequencies of the body motion, the mass of the wings is much smaller than the body mass, and the upstroke and downstroke motions of the wings are symmetric, the wingbeat-cycle average technique may be used to reform Eqs. (13) and (14):

$$ {}_b\bar{\mathbf{F}}_A + m\,{}_b\mathbf{g} = m({}_b\dot{\bar{\mathbf{V}}}_{cg} + {}_b\bar{\boldsymbol{\omega}}_{bd} \times {}_b\bar{\mathbf{V}}_{cg}) \quad (15) $$

$$ {}_b\bar{\mathbf{M}}_A = {}_b\bar{\boldsymbol{\omega}}_{bd} \times ({}_b\mathbf{I}_{bd}\,{}_b\bar{\boldsymbol{\omega}}_{bd}) + {}_b\mathbf{I}_{bd}\,{}_b\dot{\bar{\boldsymbol{\omega}}}_{bd} \quad (16) $$

Here, the over-bar refers to the wingbeat-cycle average values.

If the insect model is slightly deflected from its trimmed state, the equations of motion could be linearized. In the present study, the nondimensional quantities are considered:

$$ m^+ = \frac{m}{\rho U S T}, \quad g^+ = \frac{gT}{U}, \quad t^+ = \frac{t}{T} \quad (17) $$

$$ I_y{}^+ = \frac{I_y}{\rho U^2 S \bar{c} T^2} $$

$$ \delta u^+ = \frac{\delta u}{U}, \quad \delta w^+ = \frac{\delta w}{U}, \quad \delta q^+ = \delta q T, $$

$$ X^+ = \frac{X}{\rho U S}, \quad Z^+ = \frac{Z}{\rho U S}, \quad M^+ = \frac{M}{\rho U S \bar{c}} $$

where, U is the mean velocity of the wing; S is the total area of the two wings; T is the flapping period; $\bar{c}$ is the mean wing chord; X and Z are the aerodynamic forces in the x_b and z_b directions, respectively; M is the pitch moment; u and w are the velocities in the x_b and z_b directions, respectively; q is the pitch rate pf the body.

The linearized equations of motion could be given as [7]

$$\begin{bmatrix} \delta\dot{u}^+ \\ \delta\dot{w}^+ \\ \delta\dot{q}^+ \\ \delta\dot{\Theta} \end{bmatrix} = \boldsymbol{A}^+ \begin{bmatrix} \delta u^+ \\ \delta w^+ \\ \delta q^+ \\ \delta\Theta \end{bmatrix} \tag{18}$$

where, Θ is the pitch angle and

$$\boldsymbol{A}^+ = \begin{bmatrix} \frac{X_u^+}{m^+} & \frac{X_w^+}{m^+} & \frac{X_q^+}{m^+} & -g^+ \\ \frac{Z_u^+}{m^+} & \frac{Z_w^+}{m^+} & \frac{Z_q^+}{m^+} + u_e^+ & 0 \\ \frac{M_u^+}{I_y^+} & \frac{M_w^+}{I_y^+} & \frac{M_q^+}{I_y^+} & 0 \\ 0 & 0 & 1 & 0 \end{bmatrix} \tag{19}$$

Here, u_e is the flight speed.

3 Results and Discussion

3.1 Effects of the Body Aerodynamics on the Trim Conditions

The trim conditions of the insect model at various flight speeds ranging from 0.0 m/s to 4.0 m/s are derived using the trim search algorithm. The values of the three parameters f, $\bar{\phi}$, and $\bar{\alpha}$ in the trim conditions with respect to the models with and without the contribution of the body aerodynamics are presented in Table 1 against the flight speed.

In Table 1, the values in parentheses are corresponding to the model considering the contribution of the body aerodynamics. As revealed by Table 1, the difference in the mean sweep angle $\bar{\phi}$ is the most significant. According to Kim and Han [12], $\bar{\phi}$ and $\bar{\alpha}$ are effective control inputs to the pitch moment and the drag force, respectively. The flapping frequency f is believed to be the most effective to the lift force. The insect body is streamlined; therefore, its lift and drag forces should be small and have little effects on the overall aerodynamic loads of the model. Therefore, the insect does not need to significantly adjust its frequency f and rotation angle α. However, the pitch moment of the streamlined body is not small at high-speed flight, and this relatively large pitch moment resulted in a considerable adjustment of the sweep angle ϕ. As seen in Table 1, the change of $\bar{\phi}$ increases from -0.19 deg in hovering to 3.43 deg at 4.0 m/s. Therefore, we can conclude that the effects of the body aerodynamics on the trim conditions are negligible in hovering and low-speed flight, and they tend to increase with the flight speed and become considerable in fast flight.

Table1. Trimmed flight parameters

u_e, m/s	f, Hz	$\bar{\phi}$, deg	$\bar{\alpha}$, deg
0.0	27.11 (27.16)	-7.22 (-7.41)	93.14 (93.04)
1.0	25.63 (25.67)	-5.24 (-4.91)	87.30 (87.20)
2.0	23.43 (23.39)	-11.69 (-10.90)	79.92 (79.78)
3.0	26.92 (26.85)	-20.24 (-18.75)	68.32 (68.08)
4.0	24.70 (24.68)	-19.89 (-16.46)	69.06 (68.60)

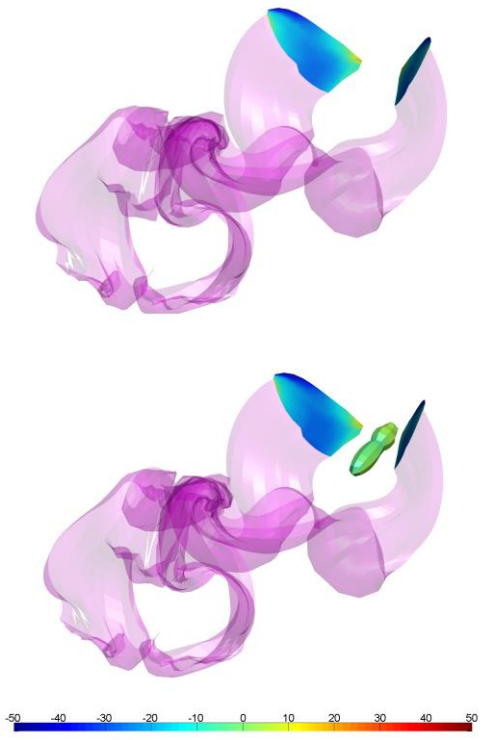

Fig. 2. Pressure differences and wake patterns at 4.0 m/s

Figure 2 illustrates the pressure differences and the wake patterns of the aerodynamic models with and without the body aerodynamics in trimmed flight at 4.0 m/s. In this figure, the color contours on the wings represents the pressure differences (in Pascal) between the lower and upper surfaces; whereas, the color contour on the body represents the differences between the far-field pressure and the pressure on the body surface [Eq. (11)].

3.1 Effects of the Body Aerodynamics on the Dynamic Stability Characteristics

The dynamic stability characteristics of insect flight could be studied through its eigenvalues and eigenvectors of the linearized dynamic system. Stability derivatives are computed and substituted into the expression of $\boldsymbol{A}^+$ in Eq. (19). The eigenvalues and eigenvectors of $\boldsymbol{A}^+$ are then derived. Figure 3 shows the eigenvalues of the dynamic systems with and without the body aerodynamics.

In Fig. 3, the blues and red markers represent the solutions corresponding to the models without and with the body aerodynamics, respectively. The green arrows show the movements of the eigenvalues when the body aerodynamics is included. It is seen that these movements become more evident at higher flight speeds. In the current flight speed range from 0.0 m/s to 4.0 m/s, the modal structure always consists of three modes, including the stable fast subsidence mode, the stable slow subsidence mode, and the unstable oscillatory mode. It is also indicated that the stable fast subsidence mode becomes more stable; while the unstable oscillatory mode becomes more unstable when the body aerodynamics is included. The stable slow subsidence mode does not seem to be affected so much by the body aerodynamics.

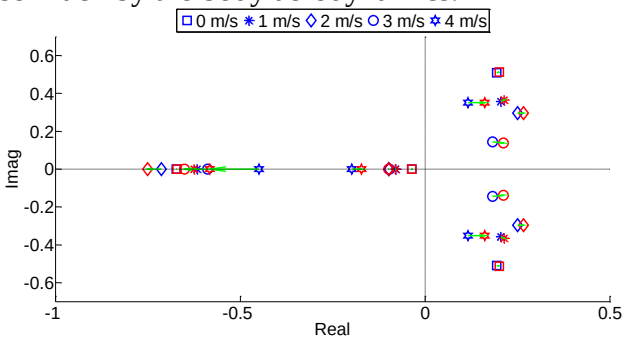

Fig. 3. Eigenvalues at various flight speeds

Table 2. Eigenvectors at 4.0 m/s

States	Mode 1	Mode 2	Mode 3
δu^+	-0.2822 ± 0.4488i (-0.2995 ± 0.3954i)	0.7990 (0.5129)	-0.3298 (0.3659)
δw^+	1.0976 ± 0.4784i (1.1155 ± 0.4201i)	4.1556 (3.1229)	-6.6332 (-4.4910)
δq^+	0.1168 ± 0.3519i (0.1622 ± 0.3509i)	-0.4491 (-0.5823)	-0.1983 (-0.1722)
$\delta\Theta$	1.0000 (1.0000)	1.0000 (1.0000)	1.0000 (1.0000)

Corresponding to the changes in the eigenvalues, the eigenvectors of the modal structure are also affected by the inclusion of the body aerodynamics. The changes of the eigenvectors at 4.0 m/s are shown in Table 2. In this table, modes 1, 2, and 3 are corresponding to the stable fast subsidence mode, the stable slow subsidence mode, and the unstable oscillatory mode, respectively. The values in parentheses are corresponding to the model with the body aerodynamics.

In general, the effects of the body aerodynamics on the longitudinal dynamic stability of the insect model increase with the flight speed, and they are considerable only at high-speed flight.

4 Conclusions

This paper has provided the numerical results and discussion regarding the effects of the body aerodynamics on the longitudinal dynamic flight stability of an insect model. To simulate insect flight, the aerodynamic model, which comprises the panel method and the extended unsteady vortex-lattice method, was coupled with the multibody dynamics code running in the *MSC. Adams* simulation environment. The trim conditions were derived by the trim search algorithm. It was shown that the effects of the body aerodynamics on the trim conditions, and on the dynamic stability characteristics are negligible in hovering and low-speed flight. However, these effects become more important when the flight speed increases. Regarding the trim conditions, the sweep angle is affected most when the body aerodynamics is considered in the computation; whereas other parameters of the wing kinematics are not affected significantly. For the modal structure of the

dynamic system, it was observed that the inclusion of the body aerodynamics results in the more stable fast subsidence mode; while the unstable oscillatory mode becomes more unstable. On the whole, the contribution of the body aerodynamics could be ignored when we study hovering and low-speed flight; however, regarding fast flight, it is important to consider this contribution.

References

[1] Sun M, Wang J and Xiong Y. Dynamic flight stability of hovering insects. *Acta Mechanica Sinica*, Vol. 23, No. 3, pp 231-246, 2007.

[2] Pfeiffer A T, Lee J-S, Han J-H and Baier H. Ornithopter flight simulation based on flexible multi-body dynamics. *Journal of Bionic Engineering*, Vol. 7, No. 1, pp 102-111, 2010.

[3] Lee J-S, Kim J-K, Kim D-K and Han J-H. Longitudinal flight dynamics of bioinspired ornithopter considering fluid-structure interaction. *Journal of Guidance, Control, and Dynamics*, Vol. 34, No. 3, pp 667-677, 2011.

[4] Cheng B and Deng X. Translational and rotational damping of flapping flight and its dynamics and stability at hovering. *IEEE Transactions on Robotics*, Vol. 27, No. 5, pp 849-864, 2011.

[5] Kim J-K, Lee J-S, and Han J-H. Passive longitudinal stability in ornithopter flight. *Journal of Guidance, Control, and Dynamics*, Vol. 35, No. 2, pp 669-674, 2012.

[6] Kim J-K and Han J-H. A multibody approach for 6-DOF flight dynamics and stability analysis of the hawkmoth Manduca sexta. *Bioinspiration & Biomimetics*, Vol. 9, No. 1, 21 pp, 2014.

[7] Kim J-K, Han J-S, Lee J-S and Han J-H. Hovering and forward flight of the hawkmoth Manduca sexta: trim search and 6-DOF dynamic stability characterization. *Bioinspiration & Biomimetics*, Vol. 10, No. 5, 20 pp, 2015.

[8] Nguyen A T, Kim J-K, Han J-S and Han J-H. Extended unsteady vortex-lattice method for insect flapping wings. *Journal of Aircraft*, doi: 10.2514/1.C033456, 10pp, 2016.

[9] Willmott A P**.** *The mechanics of hawkmoth flight*. Ph.D. dissertation, University of Cambridge, 1995.

[10] Katz J and Plotkin A**.** *Low-speed aerodynamics. From wing theory to panel methods*. 2nd edition, Cambridge University Press, 2001.

[11] Dudley R**.** *The biomechanics of insect flight*. Princeton University Press, 2000.

[12] Kim J-K and Han J-H. Control effectiveness analysis of the hawkmoth Manduca sexta: a multibody dynamics approach. *International Journal of Aeronautical and Space Sciences*, Vol. 14, No. 2, pp 152-161, 2013.

Contact Author Email Address

anhtuan@kaist.ac.kr

Copyright Statement